Supporting Information

Capotondo et al. 10.1073/pnas.1205858109

SI Materials and Methods

HSPC Double Labeling with SPIO and GFP-LV Transduction. Double labeling of HSPCs was performed coupling the GFP-LV transduction to the superparamagnetic iron oxide (SPIO) labeling. Transduction at MOI 100 was performed for 6 h after HSPC isolation. The cells, upon extensive washing in PBS, were then labeled overnight at 37 °C (4×10^6 cells per mL) with complexes made of the SPIO particles Resovist (Fe) (150 μg/mL) (SHU 555A, particle size 62 nm, Ferucarbotran, 27.9 μg Fe/mL; Schering) and Protamine sulfate (Pro) (5 μg/mL) (American Pharmaceuticals Partner; stock solution of 50 mg in 5 mL saline solution). The Fe–Pro complexes before use were incubated for 2 h on the wheel. The day after, the cells were washed by using a PBS-heparin solution (10 U/mL) to remove the residual complexes, which remain on the cell surface (1) and then used for in vitro and in vivo studies. To determine the double-labeling efficiency after washing, the cells were analyzed by MRI (see below) for iron content, by cytofluorimetry for GFP expression, and by histology. For the last analysis, the cells were transferred to cytospin slides and fixed in 4% paraformaldehyde (PFA) (Sigma-Aldrich Italia). GFP immunofluorescence (Rabbit anti GFP; Invitrogen; 1:100) was performed before Prussian blue staining, and the latter was done by using Pearls' reagent [4% potassium ferrocyanide (wt/vol) and 12% HCl (vol/vol)] for 1 h. DAPI (Roche) 1:30 in PBS was used for the detection of nuclei.

MRI Studies and Histology. ***Phantom studies and relaxometry.*** For in vitro MR imaging, 10 to 10^5 labeled or unlabeled cells were inserted in 1% low-melting agarose (SeaPlaque GTG Agarose; Lonza Rockland) blocks that were prepared in 48-cell culture wells (Corning) (Fig. S1). Fast Spin Echo T2 [repetition time (TR) 3,595 ms, echo time (TE) 96 ms, thickness 0.75 mm] and Gradient Echo T2* (TR 600 ms, TE 23 ms, flip angle 32°, thickness 0.8 mm) images were acquired in a human-grade 1.5 T MR scanner (Intera 1.5 T; Philips Medical System) by using a 23-mm circular coil. For MR relaxometry studies, 2.5×10^5, 5×10^5, or 10^6 labeled cells were resuspended in 500 μL of 4% gelatin (Sigma-Aldrich). To obtain T2 relaxometry (R2), a spinecho-multiecho sequence (TR 2,500 ms, thickness 1 mm) with eight echo times ranging between 50 and 400 ms was acquired and reconstructions of T2 maps obtained by interpolating the signal curve for the different echo times. R2 rate was calculated as 1/T2.
Ex vivo brain MR imaging. One, 5, and 14 d after transplantation of SPIO-labeled cells, mice were euthanized with lethal injection of avertin (tribromoetanolo) and extensive intracardiac perfusion with cold PBS for 15 min after clumping the femur, followed by 10 min of perfusion with 4% PFA in PBS. Brains were then collected and inserted in a plastic tube filled with 2.5% agarose (Sigma-Aldrich). The ex vivo imaging was then performed on human 1.5 or 3 T human scanners (Intera 1.5 or 3 T; Philips Medical Systems) equipped, respectively, a circular 23-mm coil and commercially available volume coil of 40 mm in diameter (Mouse Coil 3T; Philips Medical Systems). A 3D susceptibility weighted sequence (TR 480, TE 40, flip angle 20°, thickness 0.1 mm) and a 3D TSE T2 sequence (TR 3,880, TE 90, thickness 0.15 mm) were acquired.
Prussian blue staining. After MR imaging, brains from animals transplanted with SPIO-labeled HSPCs and untreated controls were serially cut in the coronal plane on a cryostat in 15-μm sections or on a vibratome in 40-μm sections. Brain sections obtained from animals transplanted with SPIO-labeled HSPCs and untreated controls were stained by using Pearls' reagent (4% potassium ferrocyanide/12% HCl, 50:50 vol/vol) for 1 h. In some experiments, nuclei were counterstained with Nuclear Fast Red (Sigma). Samples were observed in light microscopy. GFP immunofluorescence (see below) was performed before Prussian blue staining when the two stainings were analyzed together. Slides were washed in PBS, briefly air dried, and mounted with Fluorsave Reagent (Calbiochem).

Mouse Tissue Collection and Processing for Cytofluorimetry and Histology. According to the time and the group of animals described, mice were euthanized under deep anesthesia by extensive intracardiac perfusion with cold PBS for 15 min after clumping the femur. Organs were then collected and differentially processed. Bone marrow (BM) cells were collected from the clumped femur as described (2). Total cells from the liver were obtained by mechanic disgregation in PBS with 2% FBS (FBS) (BioSera); the hematopoietic cells were then isolated by density gradient using Percoll reagent (Sigma) as described (3). Brain was removed, and the two hemispheres were differently processed. For immunofluorescence analysis, one hemisphere was fixed for 24 h in 4% PFA, embedded in OCT compound, and stored at −80 °C, after equilibration in sucrose gradients (from 10 to 30%). For the flow cytometric analysis, cells from the other hemisphere were mechanically disagregated to obtain a single-cell suspension in 20 mL of GKN/BSA buffer (8 g/L NaCl, 0.4 g/L KCl, 1.42 g/L NaH_2PO_4, 0.93 g/L NaH_2PO_4, and 2 g/L D+ glucose, pH 7.4 + 0.002% BSA), without performing myeloid cell separation by Percoll gradient to preserve antigen expression on the cell surface (4). A little piece of the midbrain was stored at −80 °C for further RNA extraction.

Annexin V Staining. Annexin V staining was performed according to the manufacturer's protocol: "Annexin V-PE Apoptosis Detection Kit" (Beckton Dickinson); and 7-AAD (1 mg/mL) (Sigma-Aldrich) was also added before analysis for dead cell exclusion.

Edu Staining. EdU (5-ethynyl-2′-deoxyuridine, Invitrogen) (100 mg/kg) was administered i.p. twice a day for two consecutive days. Mice were analyzed 16 h from the last EdU injection. EdU staining was conducted by using the "Click-iTTM EdU Flow Cytometry Assay Kit" (Invitrogen) according to the manufacturer's protocol that we adapted for the analysis of brain cells. BM and liver cells were analyzed on a FACS Canto II, 3-laser (4-2-2 configuration) analyzer (Becton Dickinson), whereas brain cells were analyzed on a LSRII 4-laser analyzer (Becton Dickinson).

KSL Cell Isolation. The KSL cell fraction was isolated from Lin^- cells upon staining with the antibodies rat PE anti-mouse Sca-1 (BD Pharmingen) 1:100 and rat APC anti-mouse CD117 (c-kit) (BD Pharmingen) 1:100 and subsequently sorted on a Vantage DiVa cell sorter (Becton Dickinson). Both KLS cells and their not KS counterpart (c-$kit^{+/-}$$Sca\text{-}1^-$ and c-$kit^-$$Sca\text{-}1^+$) were then double-labeled by coupling the GFP-LV transduction and SPIO labeling following the same protocol applied to HSPCs (see above). Labeled KSL ($1–4 \times 10^4$ per mouse) and not KS Lin^- cells (5×10^5 per mouse) were i.v. transplanted into naive and busulfan-conditioned 2-mo-old $As2^{+/+}$ and $As2^{-/-}$ mice. In the case of long-term observation, supporting total bone marrow cells from CD45.1 donors were simultaneously injected.

Immunofluoresce Analysis. Brains were serially cut in the sagittal or coronal planes on a cryostat in 15-μm sections. Tissue slides were washed twice with PBS, air dried, and blocked with 0.3% Triton

X-100 (Sigma Aldrich, 114k0182), 2% BSA, and 10% NGS (Vector Laboratories) for 2 h. Then, sections were incubated overnight with primary antibodies diluted in PBS, 0.1% Triton X-100, 2% BSA, and 10% NGS at 4 °C as follows: rat PE or APC anti-Mouse CD45 (BD Pharmingen) 1:50; rat APC anti mouse CD11b (eBioscience) 1:50; rabbit anti Iba1(Wako) 1:100; chicken anti-GFP (Abcam) 1:250; rabbit anti-GFP (Invitrogen) 1:100; rabbit anti-mouse ki-67 (Novocastra Laboratories) 1:1,000; mouse PE anti-human CD271 (NGF Receptor) (BD Pharmingen) 1:50; and rat anti-mouse I-A/I-E (MHC class II) (BD Pharmingen) 1:100. The secondary antibodies goat IgG anti-Chicken Alexa Fluor 488, goat IgG anti-Rabbit Alexa Fluor 488, 546 or 633, goat IgG anti-Rat Alexa Fluor 546 or 633, and goat IgG anti-Mouse Alexa Fluor 546 (Molecular Probes, Invitrogen) were diluted 1:500 in the same blocking solution used for primary antibodies staining and incubated with sections for 2 h at room temperature. Nuclei were stained with ToPRO III (Molecular Probes, Invitrogen) 1:1,000 in PBS or by DAPI (Roche) 1:30 in PBS. TUNEL assay was performed according to the manufacturer's protocol for cryopreserved tissues with the "terminal deoxynucleotidyl transferase biotin-dUTP nick end labeling assay" (Roche). Slices were washed in PBS, air dried, and mounted with Fluorsafe Reagent (Calbiochem). Samples were analyzed by direct fluorescence microscope (Olympus Provis) or with a confocal microscope (Zeiss and Leica TCS SP2; Leica Microsystems Radiance 2100; Bio-Rad) (λ excitation = 488, 586, 660). Fluorescent signal was processed by Lasersharp 2000 software. Images were imported into Adobe Photoshop CS 8.0 software and processed by using automated level correction. For the reconstruction of brain sections, we used a fluorescence microscope Delta Vision Olympus Ix70 for the acquisition of the images, which were then processed by the Soft Work 3.5.0 software. Images were then imported into the Adobe Photoshop CS 8.0 software and reconstructed.

Electron Microscopy. A small segment of the brain tissue from mice transplanted with GFP-LV and SPIO double-labeled HSPCs after ex vivo MRI was removed (according to the presence of hypointense spots in the MR images and upon elimination of agarose), fixed in 2% glutaraldehyde, 1% osmium tetroxide, and embedded in Epon/araldite. Semithin (1-μm-thick) sections were stained with uranyl acetate and lead citrate and were analyzed by electron microscopy (Zeiss; CEM 902).

Electron spectroscopic imaging/electron energy loss spectroscopy (ESI/EELS) analyses were performed on the same electron microscope. Briefly, the patterns of net iron distribution were obtained by computer-assisted processing of two images collected below (651 and 683 eV) and one beyond the Fe-L3 absorption edge at 719 eV. The final iron map (coded in pseudocolors) was then superimposed on the ultrastructural organization of the same field obtained at 250 eV (i.e., at an energy loss where most of the elements contribute to the image).

Statistical Analyses. Where not differently specified, statistical analyses were made by one-way ANOVA for repeated measurements by using Bonferroni's or Dunnet's tests for post hoc analysis and by unpaired Student's *t* Test (confidence interval 95%).

To calculate the fold change of gene expression between different samples, we estimate a specific general multivariate linear model that accounts for the complex design of this RT-PCR experiment, including sample effect, gene effect, treatment effect, card effect, and interactions. The implemented model leads to a procedure equivalent to test the ΔΔCT (5). Advantages of this statistical technique with respect to standard techniques are described in recent literature (6). Estimation procedure is based on likelihood ratio test. The model is implemented in R-statistical software (version 2.10.0) (7).

RNA Extraction and Gene Expression Analysis. Total RNA was isolated from the brain of the same mice euthanized for flow cytometric and immunofluorescence analysis by using the TRI Reagent (Sigma-Aldrich). Upon quantification with NanoDrop 1000 spectrophotometer (Thermo Scientific), RNA was retrotranscribed with SuperScript III First-Strand Synthesis System for RT-PCR (Invitrogen). cDNA synthesis was performed by using for each sample 100 ng of total RNA primed with oligo(dT) and random primers by following manufacturer's instructions. cDNA was then amplified by using real-time PCR, performed with TaqMan Universal PCR Master Mix No AmpErase UNG (Applied Biosystems). We used the TaqMan Custom Array (Applied Biosystems) to measure the expression of 16 genes (13 targets, 2 endogenous housekeeping, and 1 internal control). Housekeeping genes were identified after analysis of TaqMan Array Mouse Endogenous Control (Applied Biosystems) on the bases of the average expression stability and the pairwise variations, determined by GeNorm analysis. One hundred nanograms of cDNA was loaded on each array. Real-time PCR was run for 35 cycles in standard mode by using an ABI 7900 HT apparatus (Applied Biosystems). The SDS 2.2.1 software was used to extract raw data [threshold cycle (CT) and raw fluorescence]. The difference (ΔCT) between the CT of each gene and that of the reference gene (PGK) was used to determine gene expression. A threshold of 0.02 was used for all of the genes inside the TaqMan low-density arrays. ΔΔCT, expressed as the difference between the ΔCT of each sample and the ΔCT of the reference for that gene, was calculated. We used as reference sample the group of age and genotype matched control mice. Finally, a value resulting from relative gene expression analysis was expressed by the 2^−ΔΔCT method and expressed as fold change (8). To calculate the fold change of gene expression between different samples, we estimated the aforementioned ANCOVA model. The outcome variable is CT, and the covariates are the sample type (i.e., BU; Xsample), Detector (target gene), Plate ID, homo/WT, Mouse, Transplant ($^{+/-}$), and Replicate. These covariates have been used when appropriate. The general multiple regression formula reads as follows:

$$CT = \beta 0 + \beta 1 \cdot XSample + \beta 2 \cdot XDetector + \beta 3 \cdot XPlateID + \beta 4 \cdot XHomo + \beta 5 \cdot XMouse + \beta 6 \cdot XTransplant + \beta 7 \cdot XReplicate + \beta 8 \cdot XDetector{\cdot}Sample + \varepsilon,$$

where CT is the threshold cycle, βi are the coefficients calculated by the model that represents the impact of the respective qualitative variable Xi, and ε is the residual error. The gene used as reference is Pgk1.

LAM-PCR and Genomic Integration Site Analysis. The sequences of LAM-PCR primers and procedures for LV integration site retrieval have been described (9). Briefly, genomic DNA was extracted from total brain, Lin^- cells and inflammatory monocytes ($Gr1^+CD11b^+CD11c^-CD49^-$ sorted cells from total $CD45^+$ cells selected from the spleen) of transplanted mice analyzed short- or long-term after HCT; 10–100 ng of DNA were used as template for LAM-PCR and initiated with a 50-cycle linear PCR and restriction digest using Tsp509I or HpyCH4IV and ligation of a restriction site–complementary linker cassette. The first exponential biotinylated PCR product was captured via magnetic beads and reamplified by a nested PCR. LAM-PCR products were separated by Spreadex gel electrophoresis (Elchrom Scientific) to verify the presence and number of bands. LAM PCR were shotgun cloned into the TOPO TA vector (Invitrogen) and directly sequenced by 454 pyrosequencing after a PCR reamplification using oligonucleotides with specific four to eight nucleotide sequence tags for sample identification. Sequences were validated and classified using specific PERL scripts and aligned to the human genome [freeze March 2006, University of California, Santa Cruz (UCSC)] using the UCSC BLAST genome browser (http://genome.ucsc.edu). Genes targeted by vector integrations were considered those nearest to the integration site.

Common integrations, represented in the Venn diagrams, were identified according to the identity of the trimmed sequence, the chromosome and integration locus and validated according to the number of reads (>1).

1. Sorgi FL, Bhattacharya S, Huang L (1997) Protamine sulfate enhances lipid-mediated gene transfer. *Gene Ther* 4:961–968.
2. Biffi A, et al. (2006) Gene therapy of metachromatic leukodystrophy reverses neurological damage and deficits in mice. *J Clin Invest* 116:3070–3082.
3. Plati T, et al. (2009) Development and maturation of invariant NKT cells in the presence of lysosomal engulfment. *Eur J Immunol* 39:2748–2754.
4. Sedgwick JD, et al. (1991) Isolation and direct characterization of resident microglial cells from the normal and inflamed central nervous system. *Proc Natl Acad Sci USA* 88: 7438–7442.
5. Yuan JS, Reed A, Chen F, Stewart CN, Jr. (2006) Statistical analysis of real-time PCR data. *BMC Bioinformatics* 7:85.
6. Pucci F, et al. (2009) A distinguishing gene signature shared by tumor-infiltrating Tie2-expressing monocytes, blood "resident" monocytes, and embryonic macrophages suggests common functions and developmental relationships. *Blood* 114:901–914.
7. R Development Core Team (2009) A language and environment for statistical computing. (R Found Stat Comput, Vienna).
8. Livak KJ, Schmittgen TD (2001) Analysis of relative gene expression data using real-time quantitative PCR and the 2(-Delta Delta C(T)) Method. *Methods* 25: 402–408.
9. Montini E, et al. (2009) The genotoxic potential of retroviral vectors is strongly modulated by vector design and integration site selection in a mouse model of HSC gene therapy. *J Clin Invest* 119:964–975.

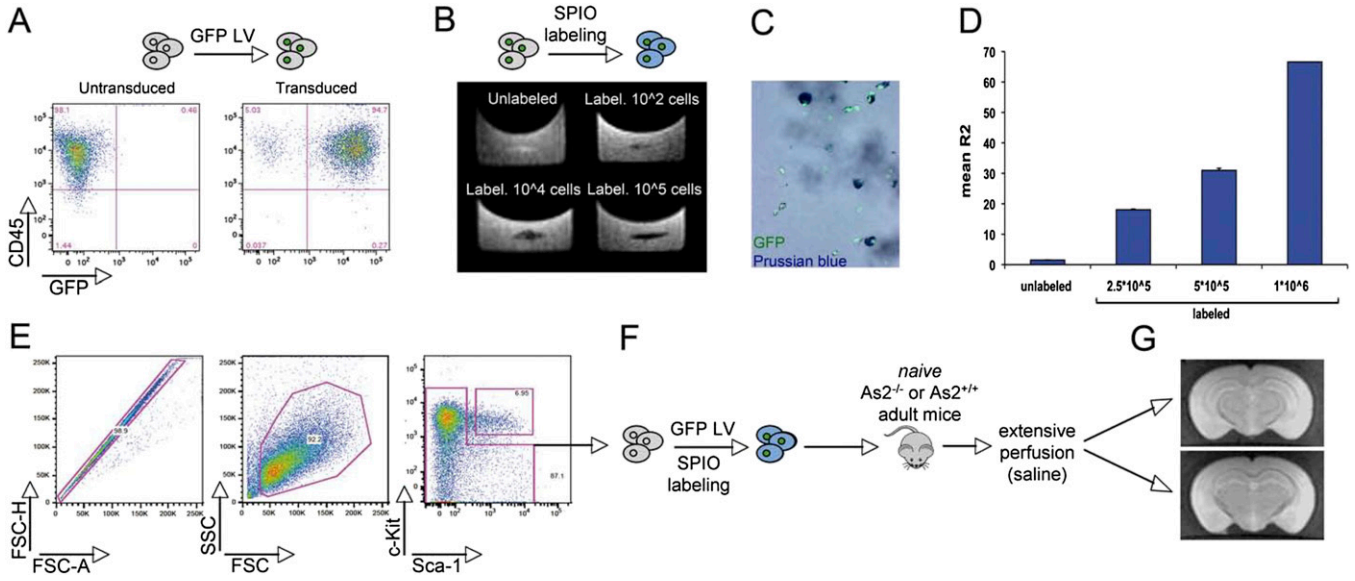

Fig. S1. GFP-LV/SPIO double labeling of HSPCs. We labeled HSPCs by 6 h transduction with GFP-LV and then by overnight incubation in medium with a combination of ferumcarbotran resovist and protamine sulfate (150 μg of Fe/mL + 5 μg/mL of protamine). (*A* and *B*) The efficiency of the double labeling was assessed by using FACS analysis for measuring GFP expression (*A*) and MRI-based evaluation (by T2* sequences on a 1.5 T human scanner) of contrast media incorporated within cells included in agarose phantoms (as indicated) (*B*). With this labeling protocol, we could clearly detect high expression of GFP in the majority of the transduced cells (*A*) and intense hypointense signal from as low as 10^2 labeled HSPCs (*B*). (*C*) Double labeling of individual cells is shown by the detection of both iron and GFP signals (obtained by Prussian blue staining and anti-GFP immunohistochemistry, respectively) within the same cell. (Magnification: 40×; images were acquired at Direct fluorescence microscope Provis Olympus.) (*D*) SPIO labeling efficiency was also evaluated by using MR relaxometry: The R2 index allowed quantification of the iron content in the labeled cells. Average values and SD are shown; $n = 5$ per condition. (*E*) Representative dot plots showing the gating strategy used for sorting c-kit$^+$Sca-1$^+$ cells and their counterparts (c-kit$^{+/-}$Sca-1$^-$ and c-kit$^-$Sca-1$^+$, not KS), starting from Lin$^-$ cells. (*Left*) Elimination of doublets. (*Middle*) Gating according to physical parameters. (*Right*) Cell identification as described above according to Sca-1 and c-kit expression. (*F*) Not KS cells were labeled with GFP-LV and SPIO and injected in As2$^{-/-}$ and As2$^{+/+}$ naïve mice. (*G*) Short term after injection, the mice were extensively perfused and ex vivo MR imaging was performed on their brains. Representative MR images showing absence of hypointense spots in the brain parenchyma of the analyzed mice.

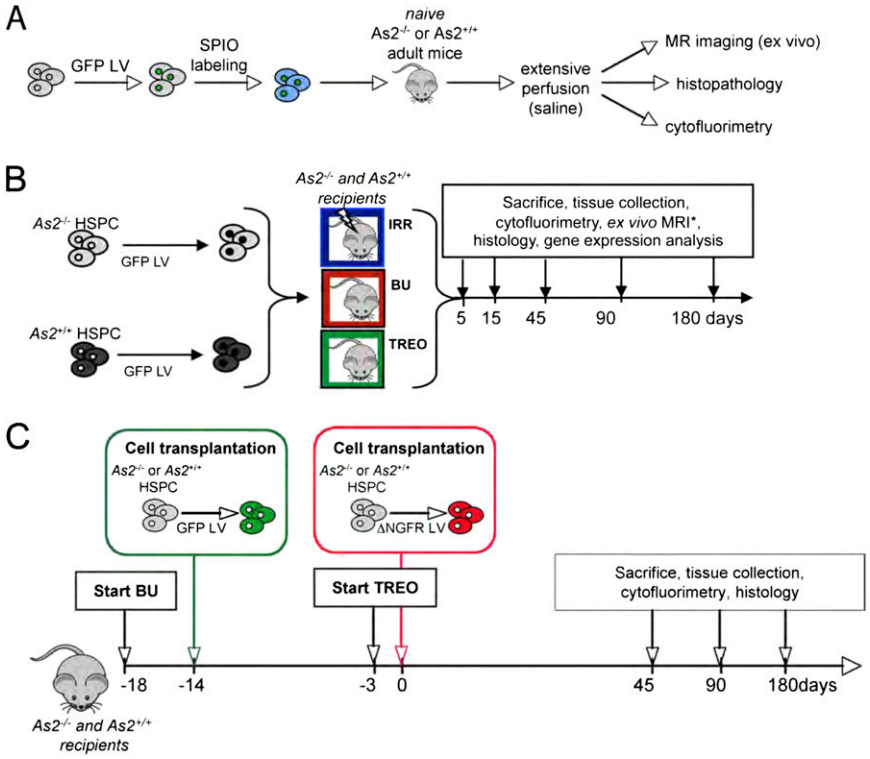

Fig. S2. Experimental schemes of transplantations as described in *Results*. Donor myeloid infiltration occurs in the brain of naïve mice (*A*), macrophage/microglia replacement in the brain of preconditioned mice (*B*), and microglia reconstitution by the donor is associated to depletion of the endogenous compartment (*C*).

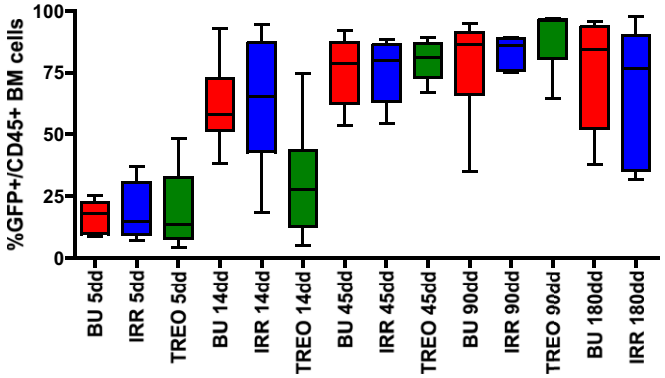

Fig. S3. Donor chimerism espressed as frequency (%) of GFP^+ cells within $CD45^+CD11b^+$ cells in the BM of transplanted mice at the indicated time-points.

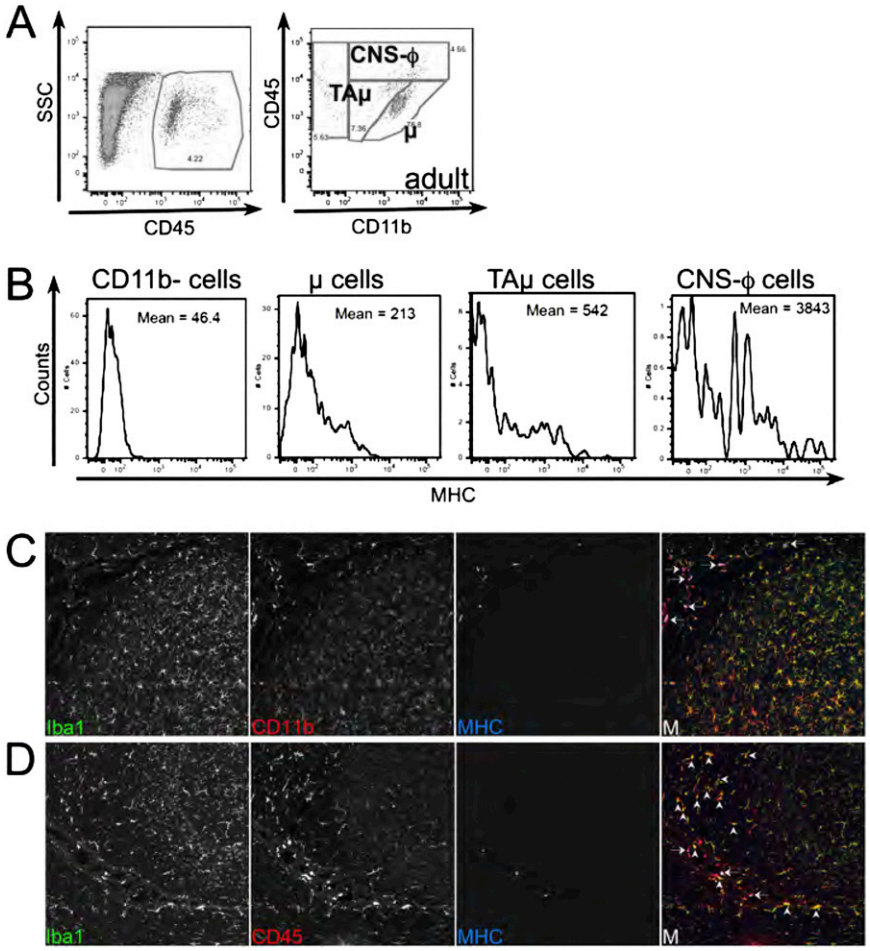

Fig. S4. Characterization of myeloid populations in the mouse brain. (*A* and *B*) Dot plots from the brain of untreated control mice of 2 mo of postnatal age showing the gating strategy used to study the brain myeloid cell compartment. The dot plots show: the total CD45^{+} hematopoietic cells within total brain cells (*A Left*) and the different subpopulations identified (*A Right*) based on the literature and our personal experience within CD45^{+} cells according to the level of expression of the CD45 and CD11b markers as follows: the CD11b$^{+/high}$CD45^{low}MHC^{-} fraction, representing mature parenchymal microglia cells (μ cells) (1–4); the CD11b^{+}CD45^{high}MHC$^{+/high}$ fraction, which represents meningeal and choroid plexus macrophages (CNS-ϕ) (4–6); the CD11b$^{+/intermediate}$CD45^{intermediate}MHC$^{-/low}$ fraction (7), which is poorly represented in adult mice, but very abundant in neonate animals and posttransplant (Fig. S7), here defined as immature and transiently amplifying microglia cells (TAμ cells) (8). The histogram in *B* shows the mean fluorescence intensity of MHC class II in each of the indicated populations. (*C* and *D*) Representative pictures from nontransplanted naïve mice showing the brain myeloid population characterized by different expression levels of the microglia/macrophage markers Iba-1, CD45, CD11b, and MHC class II. Mature microglia cells showing a highly ramified morphology with thin processes express high levels of Iba-1, low levels of CD45 and CD11b, and do not express MHC class II, consistently with the μ cell phenotype. Cells expressing high levels of Iba-1, intermediate levels of CD45, and no MHC class II and having larger cellular bodies and less and thicker ramifications are indicated by arrowheads and likely represent TAμ cells (7). Meningeal, perivascular, and choroid plexus macrophages, showing a round shape and being not ramified, express high levels of CD45, CD11b, and MHC class II (indicated by arrows) and correspond to the CNS-ϕ identified at cytofluorimetric analysis.

1. Ford AL, Goodsall AL, Hickey WF, Sedgwick JD (1995) Normal adult ramified microglia separated from other central nervous system macrophages by flow cytometric sorting. Phenotypic differences defined and direct ex vivo antigen presentation to myelin basic protein-reactive CD4+ T cells compared. *J Immunol* 154:4309–4321.
2. Carson MJ, Reilly CR, Sutcliffe JG, Lo D (1998) Mature microglia resemble immature antigen-presenting cells. *Glia* 22:72–85.
3. Ponomarev ED, Maresz K, Tan Y, Dittel BN (2007) CNS-derived interleukin-4 is essential for the regulation of autoimmune inflammation and induces a state of alternative activation in microglial cells. *J Neurosci* 27:10714–10721.
4. Hristova M, et al. (2010) Activation and deactivation of periventricular white matter phagocytes during postnatal mouse development. *Glia* 58:11–28.
5. Cruse JM, Lewis R, Dilioglou S (2004) Effects of tumor-enhancing IgG2 on macrophage function. *Exp Mol Pathol* 77:43–48.
6. Stirling DP, Yong VW (2008) Dynamics of the inflammatory response after murine spinal cord injury revealed by flow cytometry. *J Neurosci Res* 86:1944–1958.
7. Getts DR, et al. (2008) Ly6c+ "inflammatory monocytes" are microglial precursors recruited in a pathogenic manner in West Nile virus encephalitis. *J Exp Med* 205:2319–2337.
8. Hirayama M, Kuriyama M (2001) MK-801 is cytotoxic to microglia in vitro and its cytotoxicity is attenuated by glutamate, other excitotoxic agents and atropine. Possible presence of glutamate receptor and muscarinic receptor on microglia. *Brain Res* 897:204–206.

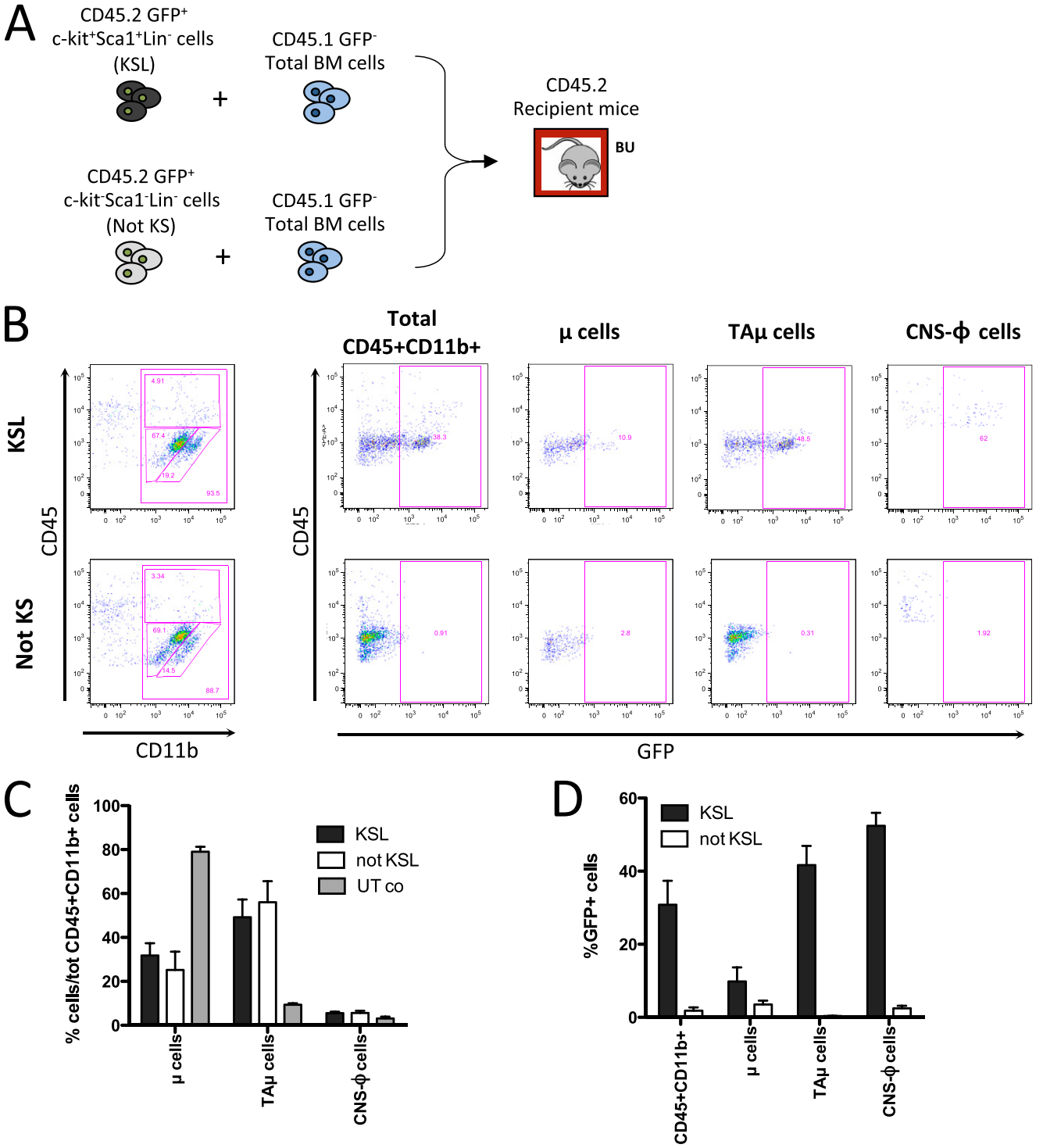

Fig. S5. Long-term evaluation of busulfan-treated animals transplanted with KSL or not KS Lin$^-$ cells. (*A*) Experimental scheme showing the transplant protocol of KSL or not KS Lin$^-$ cells into busulfan-treated CD45.2 animals (see *SI Materials and Methods* for details). (*B*) Dot plots showing the composition of brain myeloid cells in two representative busulfan-treated mice transplanted with KSL (*Upper*) or not KS Lin$^-$ (*Lower*) cells (*Left*), and the frequency of GFP$^+$ cells within each indicated brain myeloid population (*Right*). (*C*) Frequency of μ, TAμ, and CNS-ϕ cells within total CD45$^+$CD11b$^+$ brain myeloid cells of untreated control mice (UT co) and busulfan-treated mice transplanted with KSL or not KS Lin$^-$ cells. (*D*) Frequency of GFP$^+$ cells within each indicated population in busulfan-treated mice transplanted with KSL or not KS Lin$^-$ cells. *n* = 5 mice for each group. Mean and SEM are shown.

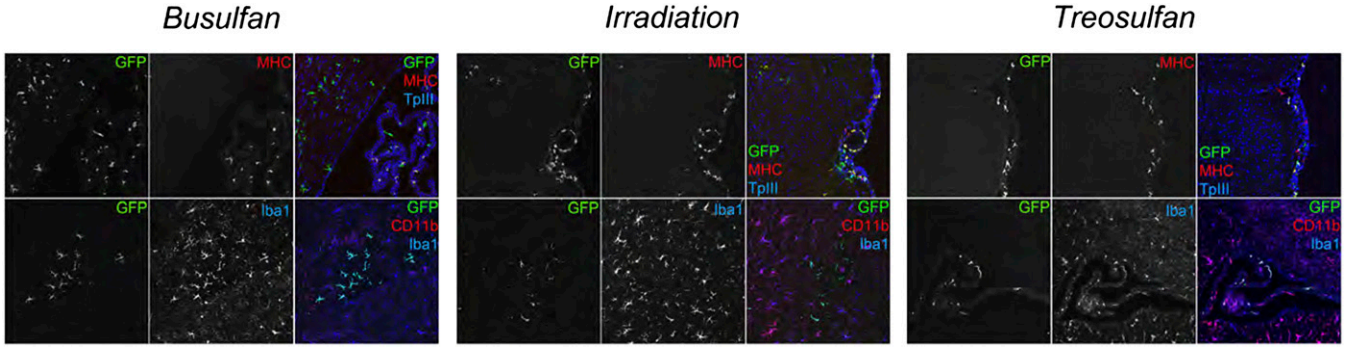

Fig. S6. Characterization of donor-derived cells in the brain of preconditioned mice. Representative pictures showing IF staining for GFP, MHC class II, Iba-1, and CD11b on brain sections from GFP$^+$HSPCs mice, treated with treosulfan, busulfan, or irradiation and analyzed at 45 d after the HCT.TPIII, nuclei. (Magnification 20×.) Images were acquired with confocal microscope Radiance 2100 (Bio-Rad).

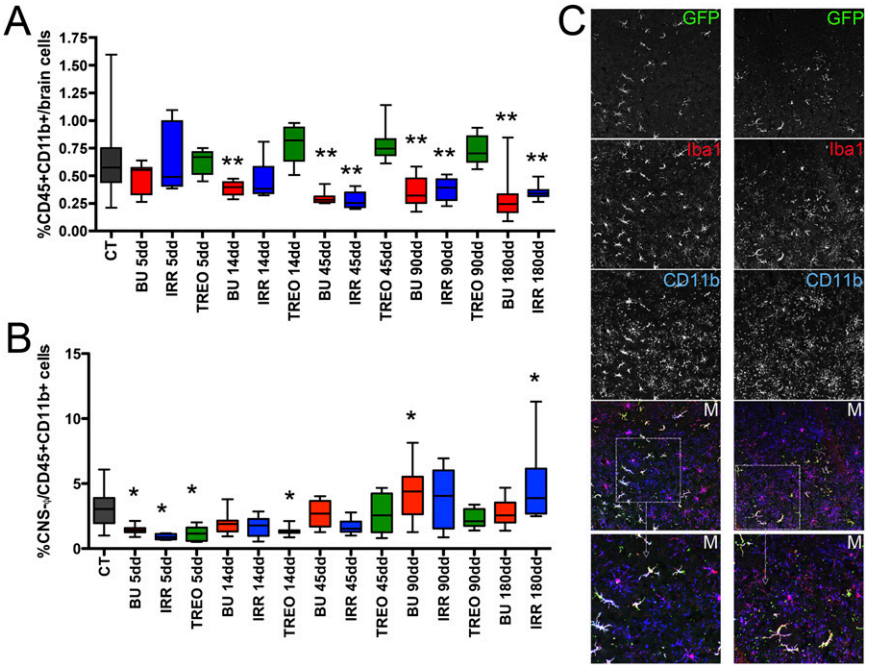

Fig. S7. Microglia reconstitution by donor cells associated to depletion of the endogenous microglia compartment. (*A* and *B*) Frequency of CD45$^+$CD11b$^+$ myeloid cells in total brain cell pool (*A*) and of CNS-ϕ (*B*) cells of pretreated and transplanted mice at different times from HCT is shown. CT, untreated mice (no conditioning, no HCT). $n \geq 10$ ($\geq$5 As2$^{+/+}$ and $\geq$5 As2$^{-/-}$) mice/group/time point. Mean and min/max values are shown. *$P < 0.05$, **$P < 0.01$ at one way Anova (Dunnet's post test). (*C*) Representative pictures showing abnormalities in the morphology of Iba-1$^+$CD11b$^+$GFP$^-$ host cells in BU-treated mice 3 mo after HCT. M, merged panels. [Magnification: *C* (*Upper*), 40×, *C* (*Lower*), 80×.]

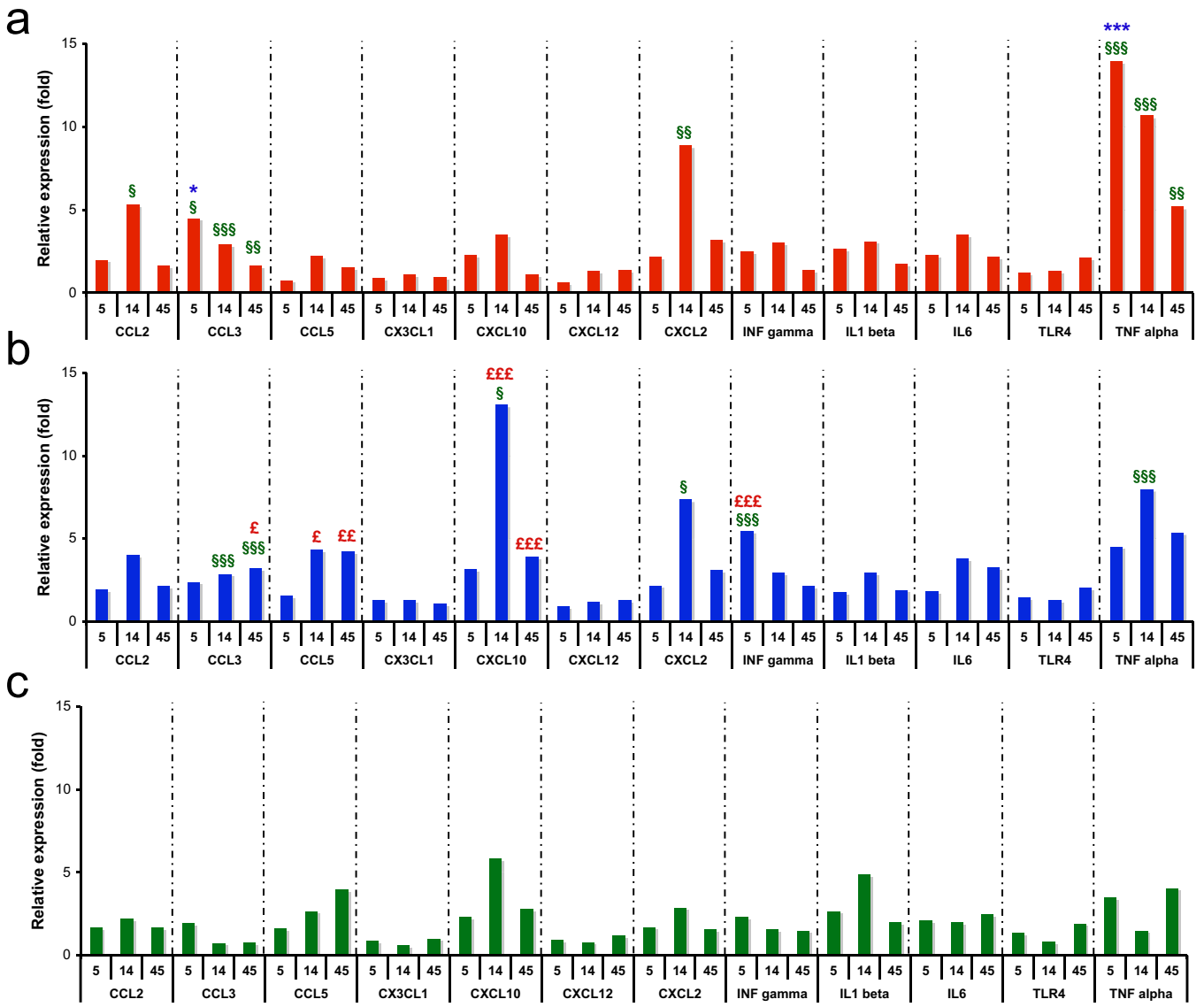

Fig. S8. Gene expression analysis on the brain of transplanted mice. Gene expression level of the indicated mRNAs in the brain of mice transplanted with LV-GFP–transduced HSPCs and analyzed at 5, 14, and 45 d after transplant. The analyzed animals represent a pool of $As2^{+/+}$ and $As2^{-/-}$ mice treated before HCT with busulfan (*A*), irradiation (*B*), and treosulfan (*C*). $n = 3$ mice per genotype for each group and time-point. Gene expression level is expressed as fold change as respect to the levels measured on a pool of age- and sex-matched untreated $As2^{-/-}$ and $As2^{+/+}$ mice. In all of the graphs, gene expression level is calculated as 2^-ΔΔCT, being ΔΔCT=ΔCT sample-ΔCT reference and ΔCT = Ct target gene-CT endogenous gene (Pgk1). Statistical analysis was performed as described in *Methods*. Statistically significant values of increased expression, comparing to each other the three conditioning regimens at each time-point, are indicated by the symbols: £, busulfan vs. the two other treatments; *, irradiation vs. the two other treatments; and §, treosulfan vs. the two other treatments; ($^{£}$, *, §) = $P < 0.05$; ($^{££}$, **, §§) = $P < 0.01$; ($^{£££}$, ***, §§§) = $P < 0.001$.

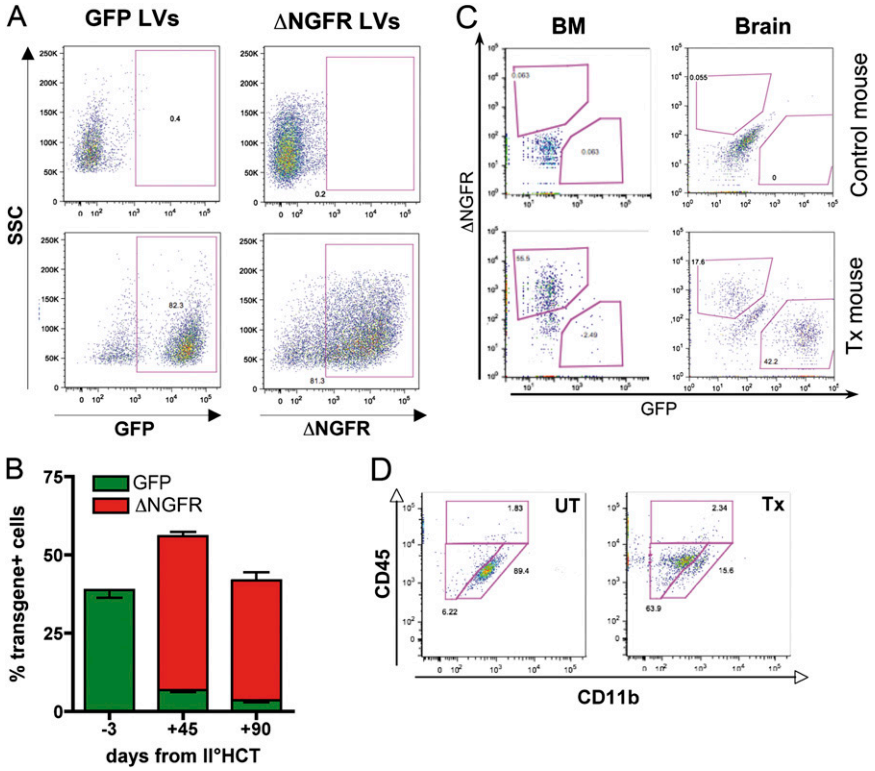

Fig. S9. Characterization of the transduced cells in the sequential transplant experiment. (*A*) Representative dot plots showing the efficiency of GFP- and ΔNGFR-LV transduction of HSPCs: untransduced cells are shown in *Upper*; transduced HSPCs in *Lower*. (*B*) Frequency of transgene$^+$ [GFP$^+$ (green) and ΔNGFR$^+$ (red)] donor-derived cells in peripheral blood mononuclear cells of mice receiving the sequential transplantation described in Fig. 5. Mean and SEM are shown. $n = 6$ mice per time-point and group. (*C*) Frequency of transgene$^+$ [GFP$^+$ (green) and DNGFR$^+$ (red)] donor-derived cells in peripheral blood mononuclear cells of mice receiving the sequential transplantation described in Fig. 6. Mean and SEM are shown. $n = 6$ mice per time-point and group. (*D*) Dot plots showing the composition of the brain myeloid cells of a representative double-transplanted mouse (Tx) analyzed 90 d after the second HCT compared with an untreated and not transplanted age-matched control (UT).

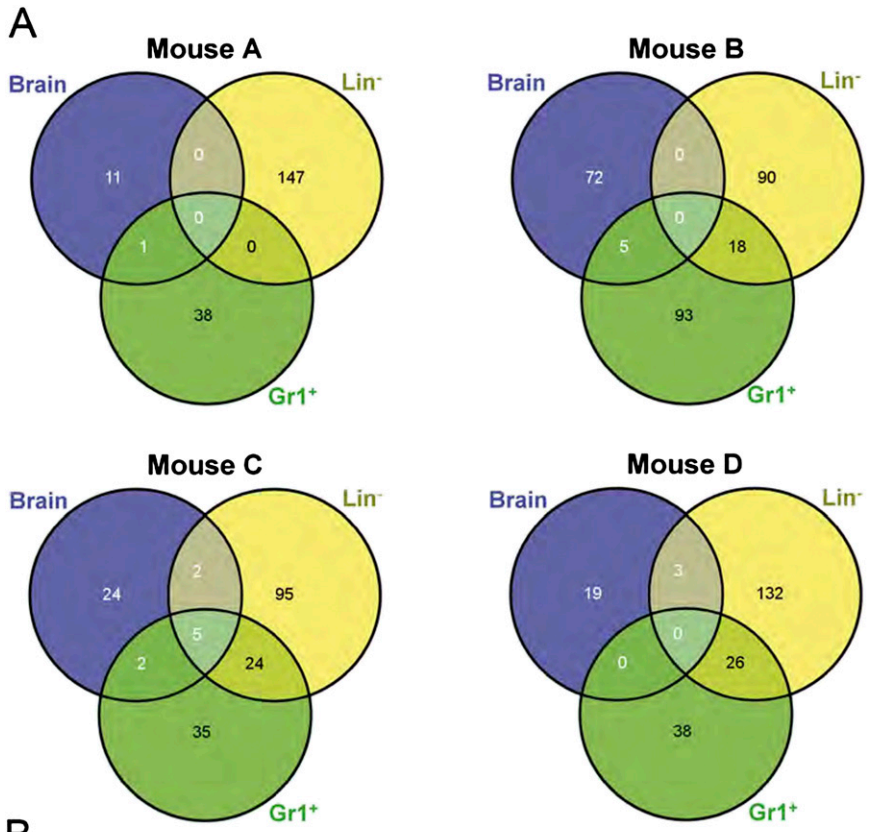

B

	Brain	Gr1+	Lin-
% integrations shared with Lin-	6.9%	25.6%	100%

Fig. S10. LV integration site analysis in the transplanted animals. To confirm the short-term homing to the brain and further local expansion of a subset of the transplanted genetically labeled HSPCs, we took advantage of the integrating nature of LVs and performed an integration site analysis. LV integration sites were retrieved from the brain, Lin^- BM cells, and spleen inflammatory monocytes ($Gr1^+CD11b^+CD11c^-CD49^-CD45^+$) of transplanted naïve or conditioned mice short and long term after HCT (Table S1). (*A* and *B*) We analyzed integration sites shared between the different samples from each individual long-term mouse. (*A*) Venn diagrams represent the common integrations shared between brain, Lin^-, and $Gr1^+$ cells retrieved from four pretreated mice analyzed 6 mo after the transplantation. (*B*) Table showing the percentage of common integrations shared between the different analyzed populations and Lin^- cells of the animals analyzed in *A* considered as a pool. The percentage was calculated as the ratio between the average of the shared integrations with Lin^- cells and of the total integrations retrieved from each cell population analyzed. The LV integrations shared between the brain myeloid cells and the Lin^- cells were much less than those shared between the inflammatory monocytes and Lin^- cells, suggesting the latter two populations to be more closely developmentally linked than the former.

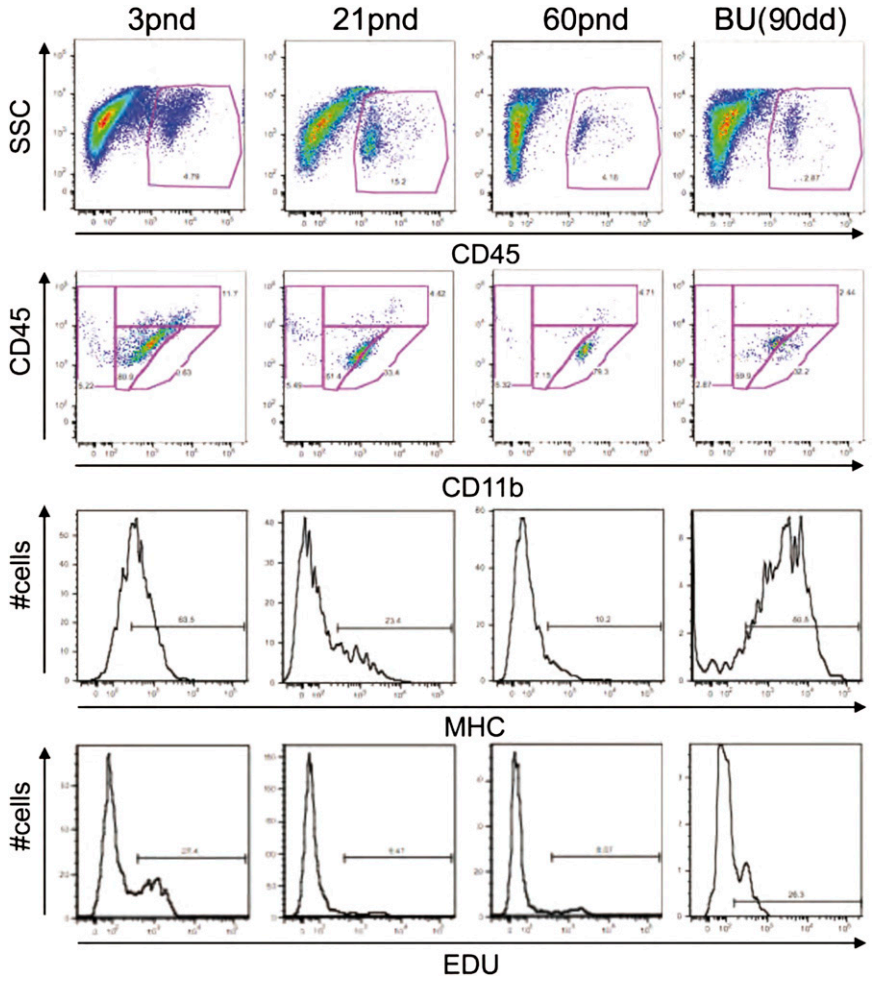

Fig. S11. Myeloid populations in the developing brain and after transplant. To better characterize the proliferating myeloid cells in the brain of the transplanted mice, we performed a comparative study. In particular, after in vivo labeling with EdU, myeloid populations were retrieved from the brain of control untreated mice at different postnatal ages and analyzed by flow cytometry in comparison with transplanted animals. Surface marker expression (CD45, CD11b, and MHC class II) and EdU proliferation after in vivo labeling of total myeloid cells ($CD45^+CD11b^+$) from the brain of naïve wild-type mice at different postnatal ages (3, 21, and 60 pnd) and in busulfan-treated and transplanted animals at 90 d from HCT are shown. At 3 d of postnatal life, brain myeloid cells are mostly composed of immature cells that could be compared with TAμ cells being $CD45^{intemediate}CD11b^+$ and expressing MHC class II at high level; during postnatal development this population showed a progressive down-regulation of CD45 and MHC class II expression and an up-regulation of CD11b expression, leading to the appearance of bona fide μ cells. Simultaneously, a progressive decrease of $CD45^+CD11b^+$ cell proliferation occurred. Interestingly, upon busulfan treatment and HCT in adult mice, $CD45^+CD11b^+$ cells showed a surface antigen profile and proliferation rate very similar to those of postnatal day 3 naïve mice, suggesting on going maturation of the myeloid population.

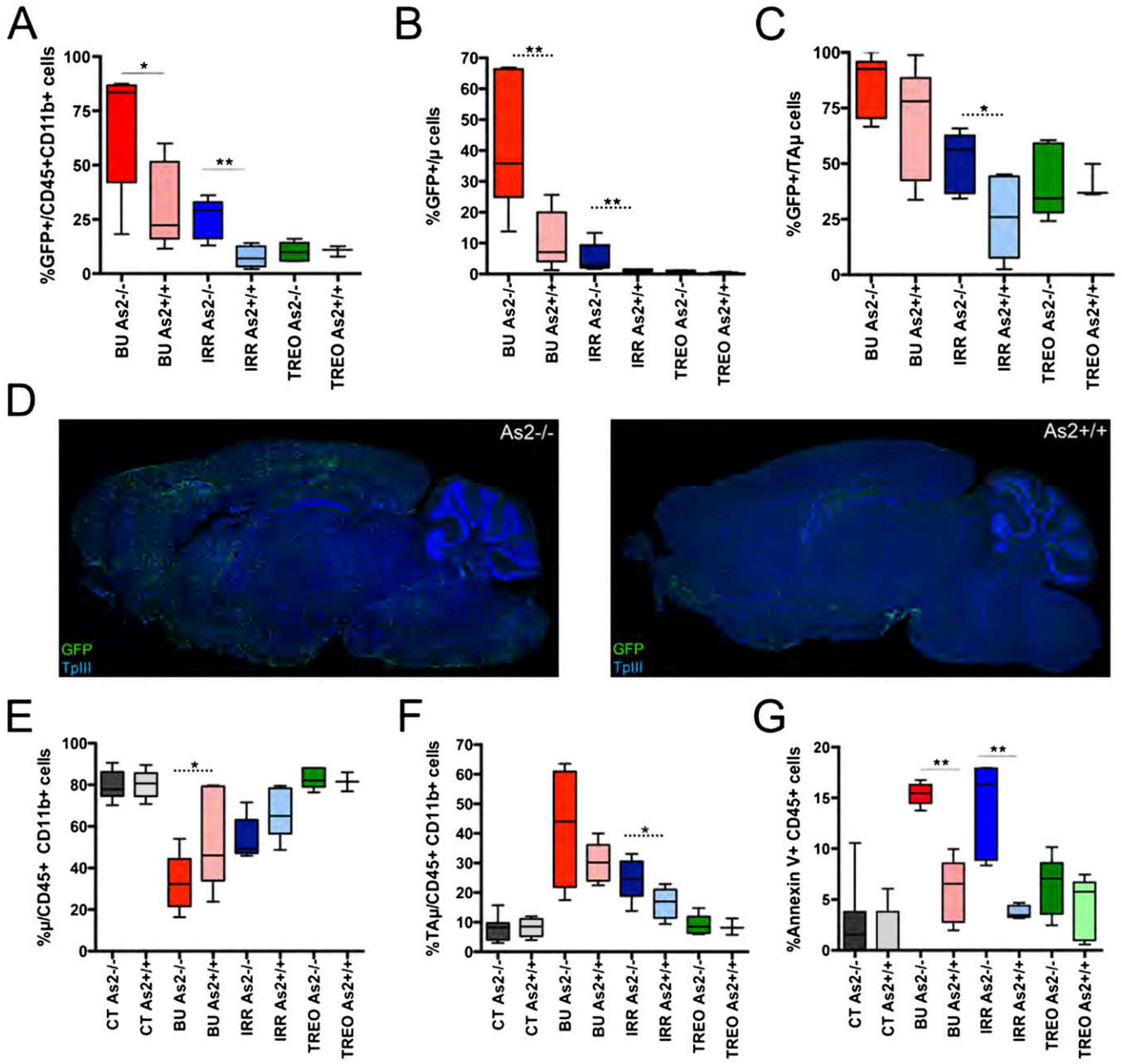

Fig. S12. Susceptibility of the disease microglia to regimen-related toxicity. We analyzed the effect of the disease on the extent of microglia reconstitution by the donor and of the depletion of the endogenous microglia compartment after HCT. (*A*–*D*) The donor GFP-expressing cells more abundantly reconstituted the myeloid brain compartment of MLD mice compared with their WT counterparts. However, this difference was noticed only when busulfan or irradiation were used for mice pretreatment. The frequency of GFP^+ cells within each different population [total $CD45^+CD11b^+$ cells (*A*), µ (*B*), and TAµ cells (*C*)] from pretreated transplanted $As2^{-/-}$ and $As2^{+/+}$ mice measured 90 d after the transplant is shown (see images for the treatment color code). (*D*) Representative pictures showing the distribution of GFP^+ cells in the brain of busulfan-treated $As2^{-/-}$ (*Left*) and $As2^{+/+}$ (*Right*) mice, 90 d after HCT are shown. GFP immunofluorescence and ToPro III for the detection of nuclei. (Magnification: 20×) Images were acquired at Delta Vision Olympus Ix70 and processed by the Soft Work 3.5.0 software, and the reconstructions were performed by using the Adobe Photoshop CS 8.0 software. (*E*–*G*) MLD mice showed more pronounced long-term depletion of microglia with expansion of TAµ cells [the frequency of µ (*E*) and TAµ (*F*) cells in the brain of pretreated transplanted $As2^{-/-}$ and $As2^{+/+}$ mice, 90 d after the transplant is shown], and greater short-term myeloid cell apoptosis compared with WT littermates upon busulfan treatment or irradiation (*G*; the frequency of Annexin V+ cells in the $CD45^+CD11b^+$ brain cells of pretreated transplanted $As2^{-/-}$ and $As2^{+/+}$ mice, 14 d after the transplant is reported), likely related to a greater sensitivity of these cells to regimen-related toxicity because of their engulfed and activated state. $n \geq 5$ $As2^{+/+}$ and ≥ 5 $As2^{-/-}$ mice for each group at each time point. Mean and min/max values are shown; $^*P < 0.05$, $^{**}P < 0.01$ at Student's *t* test (conducted within each genotype miss-matched treatment pairs).

Table S1. Analysis of vector integrations in the tissues/cells retrieved from transplanted mice

Sample	Average no. of not-redundant integrations			Average no. of individual reads		
	Brain	Lin^- cells	$Gr1^+$ cells	Brain	Lin^- cells	$Gr1^+$ cells
Naïve mice (5 d after HCT)	40	27	—	3.5	138	—
Conditioned mice (5 d after HCT)	59	714.5	—	2.5	18.5	—
Conditioned mice (6 mo after HCT)	36	135.5	70	150	28.8	50

Conditioned mice: comprises both busulfan-treated and irradiated animals (no treosulfan-treated mice). Lin^- cells were isolated from the bone marrow, $Gr1^+$ cells were isolated from the spleen as $Gr1^+CD11b^+CD11c^-CD49^-CD45^+$ cells. LV integrations were found in all examined tissues, confirming short-term homing of the genetically labeled donor cells in the brain. Interestingly: (*i*) a greater number of nonredundant integrations was retrieved short term from the BM Lin^- cells (and not from the brain) of conditioned vs. naïve mice, suggesting that short-term HSPC homing to the BM, but not to the brain, was influenced by the administration of the conditioning regimen; (*ii*) although the number of unique LV integrations in the BM decreased over time consistently with the expected loss of the infused gene-marked committed progenitors and the stable engraftment only of hematopoietic stem cells (HSCs), it remained almost stable in the brain; (*iii*) each unique integration in the brain was retrieved multiple times in the long-term analyzed animals compared with their short-term counterparts and, most importantly, compared with the BM Lin^- and spleen $Gr1^+$ cells of the same mice.